

# Trust Region Continual Learning as an Implicit Meta-Learner

Zekun Wang <sup>\*1</sup> Anant Gupta <sup>\*1</sup> Christopher J. MacLellan <sup>1</sup>

## Abstract

Continual learning aims to acquire tasks sequentially without catastrophic forgetting, yet standard strategies face a core tradeoff: regularization-based methods (e.g., EWC) can overconstrain updates when task optima are weakly overlapping, while replay-based methods can retain performance but drift due to imperfect replay. We study a hybrid perspective: *trust region continual learning* that combines generative replay with a Fisher-metric trust region constraint. We show that, under local approximations, the resulting update admits a MAML-style interpretation with a single implicit inner step: replay supplies an old-task gradient signal (query-like), while the Fisher-weighted penalty provides an efficient offline curvature shaping (support-like). This yields an emergent meta-learning property in continual learning: the model becomes an initialization that rapidly *re-converges* to prior task optima after each task transition, without explicitly optimizing a bilevel objective. Empirically, on task-incremental diffusion image generation and continual diffusion-policy control, trust region continual learning achieves the best final performance and retention, and consistently recovers early-task performance faster than EWC, replay, and continual meta-learning baselines.

## 1. Introduction

Learning is rarely stationary. Models face shifting data streams and evolving environments. Continual learning studies how to acquire new tasks sequentially while remaining robust on previously learned tasks without repeatedly retraining from scratch. However, neural networks trained with standard gradient-based updates can suffer severe catastrophic forgetting, motivating methods that explicitly stabilize old knowledge while learning new

<sup>\*</sup>Equal contribution <sup>1</sup>College of Computing, Georgia Institute of Technology, Atlanta, GA 30332, USA. Correspondence to: Zekun Wang <zekun@gatech.edu>.

Preprint. February 3, 2026.

skills. Two families of methods dominate continual learning. Regularization-based approaches preserve earlier tasks by penalizing changes to important parameters, often using Fisher-like quadratic constraints (Kirkpatrick et al., 2017; Zenke et al., 2017; Aljundi et al., 2018). Yet, they rely critically on both the existence of shared parameters across tasks and the fidelity of their curvature approximations, conditions that often fail under distribution shift or crude Fisher estimates. Replay-based approaches retain performance by interleaving current training with stored or generated past samples (Rolnick et al., 2019; Shin et al., 2017), but are limited by memory policies and can drift when generations are imperfect and bootstrapped. (Zverev et al., 2025).

A natural extension is to combine replay and regularization so that replay encourages parameter sharing while regularization constrains replay-induced drift. Recent diffusion-based generative models (Ho et al., 2020) make this combination particularly effective. Diffusion models can produce high-quality replay samples, and their gradient geometry can yield substantially improved Fisher approximations: Wang et al. (2026) shows that diffusion models admit an approximately rank-1 empirical Fisher, enabling a cheap yet informative Fisher estimate and making elastic weight consolidation (EWC, Kirkpatrick et al. (2017)) a strong complement to replay. Inspired by this line of work, we adopt a trust region view of EWC and replay synergy: EWC as a Fisher-metric trust region while replay supplies the gradient signal that drives parameter updates, analogous in spirit to trust region methods that limit steps under local Kullback–Leibler divergence (Schulman et al., 2017).

In this paper, we analyze the learning dynamics induced by such updates on diffusion models. We show that, under local approximations, the resulting update takes a MAML-style form with one inner adaptation step (Finn et al., 2017): replay supplies a query gradient on past data, while the EWC Fisher forms an efficient offline approximation to the second-order Hessian matrix on the past support set. This view links continual learning and meta-learning at the level of optimization dynamics. Even without an explicit bi-level procedure (Finn et al., 2017), the continual learning update can yield an initialization-like property that supports faster re-adaptation on prior tasks. Unlike continual meta-learning methods that begin with an explicit bi-level objective and then adapt it to sequential tasks (Finn et al., 2019; Riemer et al., 2019;

Javed & White, 2019; Gupta et al., 2020; Wu et al., 2023), we start from this continual learning objective and analyze what meta-learning structure it induces. Empirically, we test whether trust region continual learning yields *faster re-convergence* under sequential training in two regimes: (i) low-heterogeneity task-incremental diffusion image generation on ImageNet-500, and (ii) high-heterogeneity diffusion policy control on Continual-World-10. We compare against continual-learning baselines (generative replay (Masip et al., 2025), EWC with rank-1 Fisher (Kirkpatrick et al., 2017; Wang et al., 2026), and naive fine-tuning) and continual meta-learning baselines (follow the meta leader (FTML, Finn et al. (2019)), variance reduced meta-continual learning (VR-MCL, Wu et al. (2024))). Across both domains, trust region continual learning re-converges on earlier tasks faster and improves retention, supporting our claim that Fisher-metric trust region constraints can induce emergent meta-learning behavior.

Our contributions are: (i) We frame the combination of EWC and replay as trust region continual learning, where replay supplies old-task gradients and the EWC pulls updates to be near old-task optima (Kirkpatrick et al., 2017; Schulman et al., 2017); (ii) Under local approximations, we show the trust region continual learning takes a one-step MAML form, exposing an implicit meta-objective over past tasks (Finn et al., 2017); (iii) On diffusion image generation and diffusion policy control, we benchmark against EWC-only, replay-only, and continual meta-learning (Finn et al., 2019; Wu et al., 2024), showing faster early re-convergence with competitive retention. More broadly, we propose a robust, scalable, and efficient approach that bridges continual learning and meta-learning.

## 2. Related Work

### 2.1. Diffusion Models

Diffusion models define a latent-variable generative process by gradually corrupting data with a forward noising Markov chain and learning a reverse-time denoising process (Sohl-Dickstein et al., 2015; Ho et al., 2020). In the common variance-preserving formulation, the forward process is

$$q(\mathbf{x}_t \mid \mathbf{x}_{t-1}) = \mathcal{N}\left(\sqrt{1 - \beta_t} \mathbf{x}_{t-1}, \beta_t \mathbf{I}\right), \quad (1)$$

which admits the closed-form marginal

$$\mathbf{x}_t = \sqrt{\bar{\alpha}_t} \mathbf{x}_0 + \sqrt{1 - \bar{\alpha}_t} \boldsymbol{\epsilon}, \quad \boldsymbol{\epsilon} \sim \mathcal{N}(\mathbf{0}, \mathbf{I}), \quad (2)$$

where  $\alpha_t = 1 - \beta_t$  and  $\bar{\alpha}_t = \prod_{i=1}^t \alpha_i$ . The reverse model  $p_\theta(\mathbf{x}_{t-1} \mid \mathbf{x}_t)$  is typically trained via noise prediction, minimizing

$$\mathcal{L}_{\text{simple}}(\theta) = \mathbb{E}_{t, \mathbf{x}_0, \boldsymbol{\epsilon}} \left[ \|\boldsymbol{\epsilon} - \boldsymbol{\epsilon}_\theta(\mathbf{x}_t, t)\|_2^2 \right], \quad (3)$$

which is closely connected to denoising score matching (Hyvärinen, 2005; Vincent, 2011; Song et al., 2021b). Non-Markovian samplers such as DDIM further enable fast generation by modifying the reverse dynamics without retraining (Song et al., 2021a).

Beyond high-quality image synthesis, diffusion models have also proven effective for sequential decision-making. Recent work treats action trajectories as conditional generation, enabling strong results in offline RL and robot imitation/control by sampling coherent action sequences conditioned on goals and observations (Janner et al., 2022; Chi et al., 2023).

### 2.2. Continual Learning

Continual learning studies training on a stream of tasks while maintaining performance on earlier tasks, where catastrophic forgetting is a central challenge (McCloskey & Cohen, 1989; French, 1999). A major family of methods mitigates forgetting by constraining parameter drift, e.g., EWC via a Fisher-weighted quadratic penalty (Kirkpatrick et al., 2017) and synaptic intelligence via online importance estimates accumulated over training trajectories (Zenke et al., 2017). Another family relies on replay, interleaving stored examples from prior tasks with current-task updates (Rebuffi et al., 2017; Barari et al., 2026). Hybrid combinations of replay and regularization (Heng & Soh, 2023; Wang et al., 2026) also consistent with consolidation and replay perspectives from cognitive science (McClelland et al., 1995).

Generative replay replaces explicit storage of past data with a learned generator that synthesizes pseudo-samples from previous tasks, reducing memory demands and enabling flexible replay schedules (Shin et al., 2017; van de Ven & Tolias, 2019). Diffusion models are particularly attractive generators due to their high-fidelity synthesis; diffusion-based generative replay has been explored in class-incremental generation and dense prediction (Gao & Liu, 2023; Chen et al., 2023; Kim et al., 2024). Since the generator itself is continually updated, stabilizing the reverse denoising dynamics becomes important; generative distillation addresses this by distilling the reverse chain across timesteps (Masip et al., 2025). Building on this line, we study hybrid continual diffusion training that combines diffusion replay with stronger curvature approximations derived from diffusion gradients (Wang et al., 2026).

### 2.3. Meta-Learning and Continual Meta-Learning

Meta-learning (“learning to learn”) aims to acquire inductive biases from a distribution of tasks so that a model can adapt rapidly to a new task using only a few examples (Finn et al., 2017; Hospedales et al., 2020). A common formulation is bi-level optimization: for task  $\mathcal{T} \sim p(\mathcal{T})$ , an inner loop adapts parameters using task training data, and an outer loop

updates meta-parameters to minimize post-adaptation loss,

$$\begin{aligned} \min_{\theta} \mathbb{E}_{\mathcal{T} \sim p(\mathcal{T})} [\mathcal{L}_{\mathcal{T}}(\theta'^{(k)}; \mathcal{D}_{\mathcal{T}}^{\text{te}})] \\ \text{s.t. } \theta' = \theta - \alpha \nabla_{\theta} \mathcal{L}_{\mathcal{T}}(\theta; \mathcal{D}_{\mathcal{T}}^{\text{tr}}). \end{aligned} \quad (4)$$

where  $(\mathcal{D}_{\mathcal{T}}^{\text{tr}}, \mathcal{D}_{\mathcal{T}}^{\text{te}})$  denotes a task with training/test splits,  $\theta$  are the meta-parameters (initialization),  $\theta'$  are the inner-loop adapted parameters (a gradient step of size  $\alpha$  on  $\mathcal{L}_{\mathcal{T}}$ ), and  $\theta'^{(k)}$  is the adapted parameter after  $k$  such steps, whose test loss is minimized in expectation (Finn et al., 2017). Follow-up work improves scalability by avoiding higher-order derivatives (Nichol et al., 2018) or by learning the update rule itself (Li et al., 2017).

Continual meta-learning extends this paradigm to settings where tasks arrive sequentially (often with distributional shift), requiring the meta-learner to accumulate reusable knowledge while remaining adaptable. Most prior continual meta-learning methods start from an explicit meta-learning objective and adapt it to sequential task streams, often using replay, online meta-updates, or meta-regularization (Finn et al., 2019; Riemer et al., 2019; Javed & White, 2019; Gupta et al., 2020). Wu et al. (2024) further bridges meta-learning and continual learning approaches through Hessian approximation. Regularization-based continual learning typically uses fixed (often diagonal) curvature surrogates for past tasks, whereas meta-gradient updates implicitly maintain an online Hessian estimate whose variance can be reduced via improved memory sampling (Wu et al., 2024). In our analysis, EWC provides an efficient offline Fisher surrogate for this curvature, especially for diffusion models where the empirical Fisher closely tracks local Hessian structure (Wang et al., 2026). Unlike prior bi-level formulations, we start from a practical continual learning objective and analyze the meta-learning structure it already induces.

### 3. Continual Learning in Trust Regions Induces Meta-Learning

In this section, we first define our continual learning setup and where the meta-learning behavior could emerge in Section 3.1, then recast continual learning as learning within a trust region around task optima in Section 3.2, and finally reinterpret the resulting updates as a MAML-style optimization procedure in continual learning in Section 3.3.

#### 3.1. Continual Learning Problem Set-Up

In continual learning, the learner observes a stream of tasks  $\{\mathcal{T}_t\}_{t=1}^T$  sequentially. Each task  $\mathcal{T}_t$  comes with a training set  $\mathcal{D}_t^{\text{tr}}$  and a disjoint evaluation set  $\mathcal{D}_t^{\text{te}}$ . Let  $f_{\theta}$  denote the model and let  $\mathcal{L}_t(\theta; \mathcal{D})$  be the empirical loss on task  $t$  evaluated on dataset  $\mathcal{D}$ . The standard continual learning objective focuses on retention: after finishing task  $t$ , we want good performance on all tasks seen so far, e.g., low

$\frac{1}{t} \sum_{i=1}^t \mathcal{L}_i(\theta_t; \mathcal{D}_i^{\text{te}})$ , while learning the new task.

Beyond final retained performance, we study a re-convergence phenomenon: during the learning of new tasks, performance on an old task  $\mathcal{T}_i$  may drop; yet a strong continual learning solution should recover its earlier good performance quickly. We say  $\theta_t$  exhibits fast recovery on task  $\mathcal{T}_i$  if the evaluation performance returns near the task's previously achieved level using fewer update steps.

Fast recovery also means that  $\theta_t$  functions as an initialization from which few gradient steps rapidly (re-)attain good performance on old tasks. This is the same structural property optimized in gradient-based meta-learning, which finds parameters that enable fast adaptation under a fixed inner-loop rule (Finn et al., 2017). Our setting studies an analogous fast adaptation problem, but under the continual learning constraint that tasks arrive sequentially and must not be forgotten. The key difference is that traditional few-shot evaluation of meta-learning typically targets fast adaptation to new tasks drawn i.i.d. from a task distribution. In contrast, our “tasks of interest” are the previously encountered tasks, and the  $\theta_t$  must simultaneously acquire new tasks and preserve the ability to rapidly re-converge on old tasks.

#### 3.2. Continual Learning in Trust Regions

We first revisit two canonical continual learning strategies: EWC and generative replay through the lens of trust region optimization in parameter space. Throughout, let  $\theta_i^*$  denote the parameters after learning task  $\mathcal{T}_i$ , and let  $F_{\theta_i^*}^{(i)}$  be the Fisher information (evaluated at  $\theta_i^*$ ) used to quantify how sensitive task  $\mathcal{T}_i$  is to perturbations of  $\theta$ .

**EWC as a quadratic trust region around past optima.** From a Bayesian update perspective, EWC can be derived by applying a Laplacian approximation to the previous posterior around the past optimum  $\theta_i^*$ . The resulting objective for learning task  $\mathcal{T}_t$  takes the form

$$\min_{\theta} \mathcal{L}_{\mathcal{T}_t}(\theta; \mathcal{D}_t) + \frac{\lambda}{2} \sum_{i=1}^{t-1} (\theta - \theta_i^*)^\top F_{\theta_i^*}^{(i)} (\theta - \theta_i^*), \quad (5)$$

where  $\lambda > 0$  trades off plasticity and stability. Equation (5) is the Lagrangian relaxation of an explicit trust region constraint:

$$\min_{\theta} \mathcal{L}_{\mathcal{T}_t}(\theta; \mathcal{D}_t) \quad \text{s.t.} \quad \sum_{i=1}^{t-1} (\theta - \theta_i^*)^\top F_{\theta_i^*}^{(i)} (\theta - \theta_i^*) \leq \delta, \quad (6)$$

for some radius  $\delta > 0$ . Intuitively, EWC pulls updates toward an ellipsoidal neighborhood around previous task optima, penalizing movement against the directions that are deemed important by the Fisher.

In practice, forming the full  $F_{\theta_i^*}^{(i)}$  is often infeasible, and

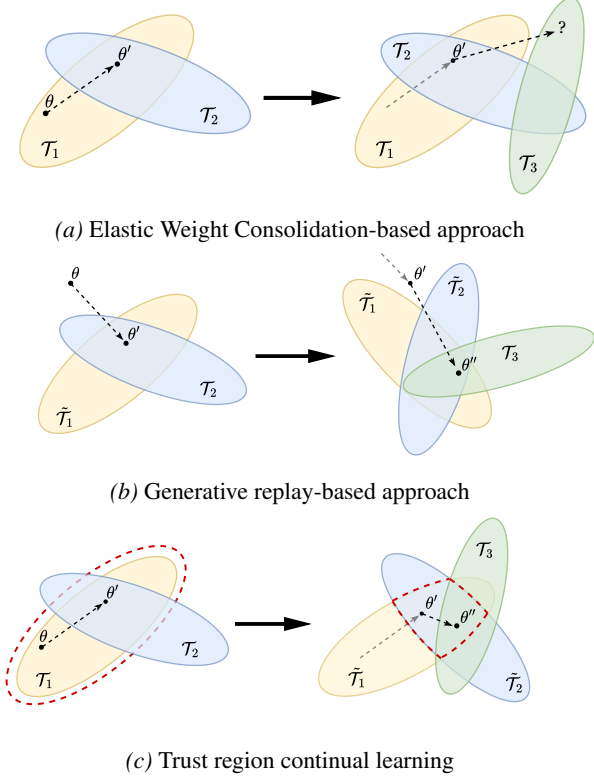


*Figure 1.* Illustrations of parameter updates when learning a new task  $T_3$  under different continual-learning strategies. Colored ellipses denote low-loss regions for each task. Dark arrows show the current update direction from  $\theta$ , and gray arrows indicate prior trajectory. (a) EWC regularizes updates toward parameters that perform well on previous tasks; if  $T_3$  has little or no overlap with earlier tasks, this constraint can yield no feasible solution (question mark). (b) Generative replay optimizes on the union of current task data and replayed samples from past tasks ( $\tilde{T}_1, \tilde{T}_2$ ), allowing convergence to a different low-loss basin, potentially far from earlier optima in overparameterized models with many equivalent solutions. (c) The hybrid approach combines replay with a trust region constraint (red dashed region), encouraging each update to remain within a neighborhood that preserves low error on previous tasks while adapting to  $T_3$ .

EWC typically uses a diagonal approximation  $F_{\theta_i^*}^{(i)} \approx \text{diag}(F_{\theta_i^*}^{(i)})$ . This simplification can be especially limiting in diffusion models where curvature may concentrate in off-diagonal structure, making diagonal constraints weak or even uninformative (Wang et al., 2026). A second limitation is geometric: if the new task optimum lies outside (or far from) the intersection of these trust regions, then the feasible set in Equation (6) can be effectively empty, yielding the failure mode illustrated in Figure 1a.

**Generative replay as optimizing on a union of task data.** Generative replay-based continual learning instead trains on a mixture of current-task data and replayed samples from past tasks. Abstractly, let  $\tilde{\mathcal{D}}_k$  denote replay data approxi-

mating task  $T_k$ . A generic replay objective is

$$\min_{\theta} \mathcal{L}_{T_t}(\theta; \mathcal{D}_t) + \beta \sum_{i=1}^{t-1} \mathcal{L}_{T_i}(\theta; \tilde{\mathcal{D}}_i), \quad (7)$$

with  $\beta \geq 0$  controlling the replay ratio.

Replay addresses EWC’s “disjoint optima” issue by explicitly encouraging solutions that perform well on the *union* of (current + replayed) data. This effectively explores shared low-dimensional data manifolds supported by all task datasets, often enabling convergence to a basin that overlaps across tasks (Figure 1b). However, replay can drift due to imperfect generators or compounding approximation error: even if the model continues to fit replayed samples, small replay mismatches can accumulate and move parameters toward a different-but-valid basin that is far from earlier optima in overparameterized networks, requiring more updates to converge to new optima.

### Trust region replay and the role of a stronger Fisher.

One can combine the complementary strengths of replay and EWC by enforcing trust region updates while replay promotes cross-task overlap:

$$\min_{\theta} \mathcal{L}_{T_t}(\theta; \mathcal{D}_t) + \beta \mathcal{L}_{\text{Replay}}(\theta) + \lambda \mathcal{L}_{\text{EWC}}. \quad (8)$$

This objective matches the geometry in Figure 1c: replay pulls optimization toward regions that remain good for previous tasks (making the trust region non-vacuous), while the Fisher-weighted penalty anchors the updates to be around past task optima.

The effectiveness of Equation (8) depends critically on the quality of  $F_{\theta_i^*}^{(i)}$ . Following Wang et al. (2026), diffusion models admit a cheap but informative Fisher approximation: in the later diffusion timesteps, per-sample gradients become strongly collinear with their mean, so the empirical Fisher is effectively rank-1. As a result, replay makes a shared basin available, while the rank-1 trust region makes movement within that basin stable by explicitly constraining the dominant curvature direction. This trust region view will be the key bridge in Section 3.3, where we reinterpret the resulting continual updates as a MAML-style optimization.

### 3.3. Reinterpretation as a MAML-style meta-learning

We now ask *what* our continual objective in Equation (8) is implicitly learning. We rewrite its optimization step and show that, under local approximations, the *old-task* part of the update takes a MAML-like form: replay provides a “query-set” gradient, while EWC provides a “support-set Hessian” constraint that shapes that gradient. Taking one

gradient step on Equation (8) yields

$$\begin{aligned} \theta \leftarrow \theta - \eta \Big( & \underbrace{\nabla_{\theta} \mathcal{L}_{\mathcal{T}_t}(\theta; \mathcal{D}_t)}_{\text{(A) current-task fit}} \\ & + \sum_{i=1}^{t-1} \underbrace{\beta \nabla_{\theta} \mathcal{L}_{\mathcal{T}_i}(\theta; \tilde{\mathcal{D}}_i)}_{\text{(B) replay / old-task query gradient}} \\ & + \sum_{i=1}^{t-1} \underbrace{\lambda F_{\theta_i^*}^{(i)}(\theta - \theta_i^*)}_{\text{(C) EWC / old-task support curvature}} \Big), \end{aligned} \quad (9)$$

where  $\eta$  is the step size,  $\tilde{\mathcal{D}}_i$  denotes generative replayed data for old task  $\mathcal{T}_i$ , and  $F_{\theta_i^*}^{(i)}$  is the empirical Fisher estimated from task  $\mathcal{T}_i$ .

For standard MAML with a single inner step ( $k = 1$ ), the adapted parameters for task  $\mathcal{T}_i$  are  $\theta'_i = \theta - \alpha \nabla_{\theta} \mathcal{L}_{\mathcal{T}_i}(\theta; \mathcal{D}_{\mathcal{T}_i}^{\text{tr}})$ . The outer update minimizes the post-adaptation (query) loss:

$$\theta \leftarrow \theta - \eta \sum_{i=1} \left( I - \alpha H_{\theta_i}^{\text{tr}} \right) \nabla_{\theta'} \mathcal{L}_{\mathcal{T}_i}(\theta'; \mathcal{D}_{\mathcal{T}_i}^{\text{te}}),$$

where  $H_{\theta_i}^{\text{tr}} = \nabla_{\theta}^2 \mathcal{L}_{\mathcal{T}_i}(\theta; \mathcal{D}_{\mathcal{T}_i}^{\text{tr}})$ . Expanding the product:

$$\begin{aligned} \theta \leftarrow \theta - \eta \Big( & \sum_{i=1} \underbrace{\nabla_{\theta'} \mathcal{L}_{\mathcal{T}_i}(\theta'; \mathcal{D}_{\mathcal{T}_i}^{\text{te}})}_{\text{(I) query gradient at adapted params}} \\ & - \sum_{i=1} \alpha \underbrace{H_{\theta_i}^{\text{tr}} \nabla_{\theta'} \mathcal{L}_{\mathcal{T}_i}(\theta'; \mathcal{D}_{\mathcal{T}_i}^{\text{te}})}_{\text{(II) support curvature correction}} \Big). \end{aligned} \quad (10)$$

The connection to MAML relies on a trust region-style observation: for many old tasks  $i < t$ , the continual update keeps  $\theta$  in a low-loss neighborhood around  $\theta_i^*$  (the low-error region in Figure 1c), so evaluating old-task gradients at  $\theta'_i$  versus at  $\theta$  makes little difference to first order (Ghorbani et al., 2019). Moreover, replayed samples provide a practical proxy for held-out performance *query/test* on old tasks. With these, evaluating the old-task query gradient at  $\theta'_i$  is well-approximated by evaluating it at  $\theta$ :

$$\text{(I)} = \nabla_{\theta'} \mathcal{L}_{\mathcal{T}_i}(\theta'; \mathcal{D}_{\mathcal{T}_i}^{\text{te}}) \approx \nabla_{\theta} \mathcal{L}_{\mathcal{T}_i}(\theta; \tilde{\mathcal{D}}_i) = \text{(B)}. \quad (11)$$

For negative likelihood-based objectives such as the diffusion ELBO (Sohl-Dickstein et al., 2015; Ho et al., 2020), the Fisher information matches the expected Hessian of the log-likelihood. Let  $\ell(\theta; x)$  denote the per-example log-likelihood and  $g(\theta; x) = -\nabla_{\theta} \ell(\theta; x)$ . Then

$$F_{\theta} = \mathbb{E}_x [g(\theta; x)g(\theta; x)^{\top}] = \mathbb{E}_x [\nabla_{\theta}^2 \ell(\theta; x)] = \mathbb{E}_x [H_{\theta}], \quad (12)$$

with a full derivation in Appendix A. In practice, MAML computes  $H_{\theta_i}^{\text{tr}}$  from mini-batches of the support set:  $H_{\theta_i}^{\text{tr}} = \mathbb{E}_{x \sim \text{batch}_{\text{tr}}} [\nabla_{\theta_i}^2 \ell(\theta_i; x)]$ . For the simplicity in notation, we

denote by  $H_{\theta_i}^{\text{tr}}$  the expected Hessian over support-set mini-batches and  $H_{\theta_i}^{\text{te}}$  analogously for query-set mini-batches.

We now connect MAML’s Hessian term (II) to the EWC term (C) using a trust region (locality) assumption. Fix an old task  $\mathcal{T}_i$  and let  $\theta_i^*$  denote the optimum after learning task  $i$ . A second-order Taylor expansion of the old-task *query* gradient around  $\theta_i^*$  gives

$$\nabla_{\theta} \mathcal{L}_{\mathcal{T}_i}(\theta; \mathcal{D}_{\mathcal{T}_i}^{\text{te}}) \approx H_{\theta_i^*}^{\text{te}}(\theta - \theta_i^*), \quad (13)$$

where  $H_{\theta_i^*}^{\text{te}}$  is the query-set Hessian. Substituting Equation (13) into (II) yields

$$H_{\theta_i}^{\text{tr}} \nabla_{\theta'} \mathcal{L}_{\mathcal{T}_i}(\theta'; \mathcal{D}_{\mathcal{T}_i}^{\text{te}}) \approx H_{\theta_i}^{\text{tr}} H_{\theta_i^*}^{\text{te}}(\theta - \theta_i^*). \quad (14)$$

Under locality, curvature varies slowly within the neighborhood, so  $H_{\theta_i}^{\text{tr}} \approx H_{\theta_i^*}^{\text{tr}}$ , consistent with observed stability of Hessian spectral outliers near converged local optima where dominant curvature directions remain consistent within local regions (Ghorbani et al., 2019). Moreover, we assume  $H_{\theta_i^*}^{\text{tr}} \approx H_{\theta_i^*}^{\text{te}}$  following the insight that the Fisher/Hessian characterizes the intrinsic geometric properties of the model’s learned predictive distribution (Martens, 2020). Consequently, the local curvature remains similar across any samples (replayed or real) that align with this underlying manifold. Finally, by Equation (12), both can be approximated by a common Fisher curvature proxy evaluated at the old optimum:

$$H_{\theta_i}^{\text{tr}} \approx H_{\theta_i^*}^{\text{tr}} \approx H_{\theta_i^*}^{\text{te}} \approx F_{\theta_i^*}^{(i)}. \quad (15)$$

Applying Equation (15) to Equation (14) gives the offline approximation

$$\text{(II)} \approx (F_{\theta_i^*}^{(i)})^2 (\theta - \theta_i^*) = \lambda F_{\theta_i^*}^{(i)}(\theta - \theta_i^*) = \text{(C)}. \quad (16)$$

When  $F_{\theta_i^*}^{(i)}$  is approximately rank-1 for diffusion models as in Wang et al. (2026),  $(F_{\theta_i^*}^{(i)})^2$  reduces to a scalar multiple of  $F_{\theta_i^*}^{(i)}$ , so Equation (16) matches the EWC form  $F_{\theta_i^*}^{(i)}(\theta - \theta_i^*)$  up to a scale factor that can be absorbed into  $\lambda$ . We provide full derivation Appendix B.

Subtitling Equations (11) and (16) to Equation (9), we have that the trust region objective is equivalent to

$$\theta \leftarrow \theta - \eta \left( \nabla_{\theta} \mathcal{L}_{\mathcal{T}_t}(\theta; \mathcal{D}_t) - \mathcal{L}_{\text{MAML}}(\theta_{i < t}) \right)$$

under local approximation.

## 4. Experimental Evaluations

We evaluate whether our continual learning approach yields *faster convergence* when training sequentially across tasks in two settings with different heterogeneity: (i) low-heterogeneity task-incremental diffusion image generation on ImageNet-500, and (ii) high-heterogeneity continual diffusion-policy control on Continual-World-10.

**Baselines.** We compare our method against three continual-learning baselines: (i) **Generative replay**, implemented via generative distillation, which has been shown effective for diffusion models (Masip et al., 2025); (ii) **EWC** (Kirkpatrick et al., 2017) using the rank-1 approximation (Wang et al., 2026); and (iii) **Naïve continual fine-tuning**, which sequentially trains on each task. To benchmark against continual meta-learning, we include **FTML**, an online extension of MAML (Finn et al., 2019), and **VR-MCL** (Wu et al., 2024). For scalability, we implement these meta-learning baselines with the standard *first-order* approximation, which typically matches second-order performance while avoiding the prohibitive cost of higher-order differentiation at our scale (Nichol et al., 2018), as our model and batch sizes are substantially larger than those in prior VR-MCL experiment setups; we provide a detailed size/computation comparison and implementation notes in the Appendix C.3. Importantly, VR-MCL’s control-variate update still reduces variance of the (first-order) stochastic meta-gradient. For meta-learning baselines, we replace experience replay with generative replay to keep the memory footprint and data-access assumptions consistent with our continual learning setting.

#### 4.1. Task-Incremental Image Generation Set-up

**Datasets and Metrics.** We use a 500-class ImageNet subset as a scaled up Tiny-ImageNet while keeping the compute footprint low (Wu et al., 2017; Russakovsky et al., 2015; Deng et al., 2009). We follow a task-incremental protocol by splitting the 500 classes into 10 disjoint tasks of 50 classes each. We evaluate with Fréchet Inception Distance (FID) (Heusel et al., 2017) on a held-out split, reporting average FID across tasks and forgetting, defined as the change in a task’s FID from when it is first learned to the end of training. We refer to Appendix C.1 for additional details.

**Implementation Details.** We train conditional diffusion models with a standard denoising diffusion objective (Ho et al., 2020; Nichol & Dhariwal, 2021) that condition on class labels. For meta-learning baselines, we split each training batch evenly into a support/query pair. We perform a single inner adaptation step so that the total number of parameter updates and the total number of training samples processed match our continual-learning setting. We refer to Appendix C.1 for model details and training configurations.

#### 4.2. Continual Robotic Manipulation Set-up

**Datasets and Metrics.** We evaluate continual robotic manipulation on Continual-World-10 (CW10) (Wołczyk et al., 2021), a 10-task sequence from Meta-World (Yu et al., 2020) (e.g., *push-wall*, *close-window*). Unlike ImageNet, CW10 spans distinct manipulation skills with different dynamics and reward conditions, and thus exhibits substantially

higher task heterogeneity. Following standard practice in Continual-World, we report the success rate for each task, defined as the fraction of evaluation rollouts that satisfy the environment’s success condition. After each task, we evaluate on all tasks seen so far using 100 trajectories per task and report average success. Forgetting is the drop in a task’s success rate from when it is first learned to the end of training. See Appendix C.2 for CW10 details.

**Implementation Details.** We instantiate the control policy as a Diffusion Policy that generates action chunks conditioned on recent observations (Chi et al., 2023). To collect expert demonstrations, we roll out scripted experts provided by the benchmark for 2500 trajectories per task, yielding an offline trajectory dataset for each task. Each training sample uses an observation horizon of 6 steps and predicts an action chunk of 2 steps, forming a sequence length of 8; we selected these values via a grid search over horizon/chunk combinations, with full results reported in Appendix C.2. For meta-learning baselines, we similarly split each training batch evenly into a support/query pair and perform a single inner adaptation step to match our continual-learning setting. We refer to Appendix C.2 for model details and training configurations.

*Table 1.* Final performance and forgetting on ImageNet-500 and CW10 with standard errors. For ImageNet, we report average FID across tasks ( $\mathcal{AFID}$ , lower is better) and average forgetting  $\mathcal{F}$  (lower is better). For CW10, we report average Success rate (SR, higher is better) and average forgetting  $\mathcal{F}$  (lower is better).

Methods	ImageNet-500		CW10	
	$\mathcal{AFID} \downarrow$	$\mathcal{F} \downarrow$	SR $\uparrow$	$\mathcal{F} \downarrow$
Finetuning	$86.2 \pm 7.3$	$50.4 \pm 7.2$	$17.9\% \pm 2.4$	$73.0 \pm 2.0$
EWC	$77.2 \pm 1.2$	$41.2 \pm 2.3$	$17.6\% \pm 1.8$	$73.7 \pm 1.3$
Replay	$53.4 \pm 6.0$	$18.2 \pm 4.6$	$85.3\% \pm 2.0$	$8.2 \pm 2.0$
FTML	$172.5 \pm 9.1$	$128.5 \pm 9.0$	$78.5\% \pm 3.8$	$13.3 \pm 3.3$
VRMCL	$142.2 \pm 8.5$	$96.6 \pm 8.4$	$77.9\% \pm 1.5$	$11.7 \pm 2.0$
Trust Region	$44.5 \pm 2.3$	$10.6 \pm 3.0$	$88.3\% \pm 0.4$	$4.4 \pm 0.9$

#### 4.3. Results and Discussions

**Trust region continual learning reduces catastrophic forgetting.** We study whether Trust Region combines the strengths of EWC and replay by comparing it to its components and finetuning across two datasets with different task heterogeneity. High task heterogeneity, such as CW10, contains meaningfully diverse manipulation tasks with varying degrees of transfer and interference, and prior analyses explicitly use transfer matrices to quantify when tasks reuse versus overwrite features (Wołczyk et al., 2021). More broadly, feature reuse and forgetting depend on task similarity: dissimilar tasks tend to transfer less and interfere more, making local constraints around old optima harder

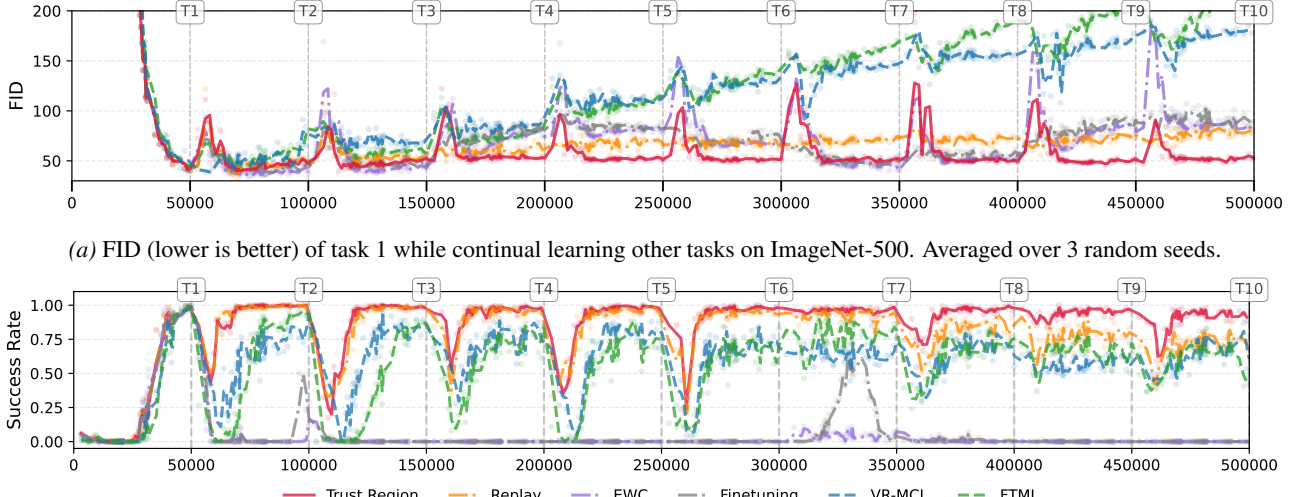


Figure 2. Task 1 performance over the course of continual training on 10 tasks, averaged over random seeds, on two datasets. Gray dashed vertical lines mark task transitions. X-axis: gradient update steps.

to satisfy (Yosinski et al., 2014; Lee et al., 2021; Goldfarb et al., 2024).

Table 1 shows that Trust Region achieves the best final performance and the lowest forgetting on both datasets. On high-heterogeneity CW10, Trust Region attains the highest average success rate ( $88.3\% \pm 0.4$ ) while also exhibiting the smallest magnitude of forgetting ( $4.4 \pm 0.9$ ), improving over replay ( $85.3\% \pm 2.0$ ,  $8.2 \pm 2.0$ ) and outperforming regularization-only baselines. EWC performs similarly to finetuning on CW10, consistent with the view that a local quadratic surrogate can be a weak guide when tasks have limited overlap (Kirkpatrick et al., 2017). Replay is competitive on CW10 because mixing past and current samples approximates multitask training over the union of tasks and thus directly supplies gradients for retention. However, generative replay can suffer from error accumulation and distribution drift when earlier generators are imperfect, which compounds over the task sequence and can worsen forgetting (Gao & Liu, 2023; Masip et al., 2025). Trust Region mitigates this by anchoring updates within a neighborhood that preserves past-task performance, improving stability relative to replay alone.

On low-heterogeneity ImageNet-500, Trust Region yields a clearer gain over replay, achieving the best average FID ( $44.5 \pm 2.3$ ) and the lowest forgetting ( $10.6 \pm 3.0$ ), improving over replay ( $53.4 \pm 6.0$ ,  $18.2 \pm 4.6$ ) and outperforming finetuning and EWC. This suggests that, even when tasks share more structure, the additional local constraint effectively helps prevent “mode hopping” across many equivalent low-loss solutions during long-horizon training in overparameterized generative models (Garipov et al., 2018; Draxler

et al., 2018).

Surprisingly, continual meta-learning baselines underperform on ImageNet-500, falling well below finetuning: FTML reaches  $172.5 \pm 9.1$  average FID with  $128.5 \pm 9.0$  forgetting, and VRMCL reaches  $142.2 \pm 8.5$  with  $96.6 \pm 8.4$  forgetting. Yet on CW10 their performance remain good, though still below Trust Region. Intuitively, lower task heterogeneity implies greater overlap among task optima, so replay-only training already tracks a shared low-loss region. Bilevel meta-learning then becomes more error-amplifying where imperfections in replay bias the outer meta-gradient objective and simultaneously corrupt the inner adaptation step taken from that slightly off initialization, pushing updates away from the shared basin (see Figure 2a). In CW10, optima overlap less and inner adaptation is less informative, so replay supplies most of the retention signal. Performance is therefore dominated by the outer meta-gradient objective, making the adaptation step comparatively less sensitive.

**Trust region continual learning recovers early-task performance faster.** To quantify how quickly early-task performance returns after learning new tasks, we measure re-convergence using the step-to-threshold metric in Table 2: after each task transition in Figure 2, we count the number of gradient updates until Task 1 returns to a target level relative to its *initial* optimum. For ImageNet-500,  $\text{FID}_1 \leq (1 + \tau)\text{FID}_1^{(0)}$  with  $\tau \in \{10\%, 20\%, 30\%\}$ , and for CW10,  $\text{SR}_1 \geq \alpha \text{SR}_1^{(0)}$  with  $\alpha \in \{99\%, 90\%, 80\%\}$ . Across tasks, these step counts typically range from single-digit to tens of updates for Trust Region methods (e.g., often recovers within  $\leq 55$  steps on ImageNet and  $\leq 45$  steps for

Method	ImageNet-500																													
	+10%										+20%										+30%									
	T2	T3	T4	T5	T6	T7	T8	T9	T10	T2	T3	T4	T5	T6	T7	T8	T9	T10	T2	T3	T4	T5	T6	T7	T8	T9	T10			
Finetune	25	45	—	—	—	—	—	—	—	5	35	—	—	—	35	50	—	—	2	25	—	—	—	25	50	—	—			
EWC	20	50	—	—	—	650	—	—	—	15	50	—	—	—	85	55	—	—	8	30	55	—	—	55	45	—	—			
Replay	30	90	—	—	—	—	—	—	—	30	75	—	—	—	—	—	—	—	2	2	5	—	—	—	—	—	—			
FTML	45	—	—	—	—	—	—	—	—	10	80	—	—	—	—	—	—	—	5	55	—	—	—	—	—	—	—			
VRMCL	4	—	—	—	—	—	—	—	—	4	—	—	—	—	—	—	—	—	4	15	—	—	—	—	—	—	—			
Trust Region	35	15	—	—	—	—	—	—	—	20	15	—	—	—	50	—	350	2	20	15	2	35	35	25	55	40	2			

Method	CW10																													
	99%										90%										80%									
	T2	T3	T4	T5	T6	T7	T8	T9	T10	T2	T3	T4	T5	T6	T7	T8	T9	T10	T2	T3	T4	T5	T6	T7	T8	T9	T10			
Finetune	—	—	—	—	—	—	—	—	—	—	—	—	—	—	—	—	—	—	—	—	—	—	—	—	—	—	—	—	—	
EWC	—	—	—	—	—	—	—	—	—	—	—	—	—	—	—	—	—	—	—	—	—	—	—	—	—	—	—	—	—	
Replay	60	95	30	80	60	30	10000	—	—	10	50	2	20	30	2	35	2	8000	10	35	2	20	15	2	4	2	45			
FTML	—	—	—	—	—	—	—	—	—	550	20000	—	3000	—	30	—	—	—	250	3000	700	800	300	2	150	900	—			
VRMCL	—	850	10000	—	—	—	—	—	—	750	650	500	250	—	—	—	—	—	400	350	100	250	85	40	550	—	30000			
Trust Region	60	80	45	70	55	50	2000	—	100	10	45	2	30	30	2	25	2	2	10	35	2	15	4	2	4	2	2			

**Table 2. Steps to re-converge Task 1 under continual learning.** Each entry reports the number of gradient updates required for Task 1 performance to return to a target level relative to its *initial* optimal Task 1 performance while the model is trained continually on later tasks. For ImageNet-500 we use FID and define targets by an allowable relative increase in Task 1 FID from its initial value (columns: +10%, +20%, +30%; i.e., reaching  $\text{FID}_1 \leq (1 + \tau)\text{FID}_1^{(0)}$ ). For CW10 we use success rate and define targets by a fraction of the initial Task 1 success (columns: 99%, 90%, 80%; i.e., reaching  $\text{SR}_1 \geq \alpha \text{SR}_1^{(0)}$ ). Missing entries are shown as “—”.

CW10 at the 90%/80% thresholds), while unstable baselines can exhibit orders of magnitude longer recovery tails (up to  $10^4$  steps) or fail to re-converge (“—”).

This behavior is informative about *where* updates live in parameter space. Replay provides gradients that keep old-task behavior “reachable,” but without an explicit locality constraint it can drift among many equivalent solutions that fit the replay mixture yet are less aligned with the original task 1 basin, requiring more steps to re-attain the previous task 1 optimum (longer recovery). Trust Region sharpens this by constraining every update to remain in a neighborhood that preserves low error on past tasks, so the model does not need to “re-learn” task 1 after each transition—it only needs a small correction to re-enter the original low-loss region (faster recovery).

The contrast is most pronounced on CW10. In Figure 2b, finetuning collapses to near-zero task 1 success on later tasks, and EWC provides little improvement, consistent with high interference where local regularization alone cannot maintain competence. We do observe occasional transfer in finetuning (e.g., a transient improvement around task 6), suggesting some shared sub-skills, but this effect is sporadic and does not prevent eventual collapse. In comparison, FTML and VR-MCL retain good task 1 performance on CW10 but recover more slowly than Trust Region after each transition, indicating that an explicit “fast-adaptation” objective does not automatically translate to fast *re-convergence* under long-horizon continual updates when replay and ini-

italization drift accumulate.

## 5. Conclusion

We presented a trust region view of hybrid continual learning that unifies generative replay and EWC: replay keeps past-task behavior reachable by providing direct training signal on previous tasks, while the Fisher-metric penalty constrains each update to remain within a neighborhood that preserves low error on earlier optima. Our analysis shows that this simple continual learning objective induces a MAML-style optimization form under local approximations, explaining why it can exhibit meta-learning-like behavior (fast re-adaptation) without an explicit bilevel procedure. Across both low-heterogeneity ImageNet-500 and high-heterogeneity CW10, this mechanism improves retention and accelerates old-task recovery: trust region attains the strongest final performance with the least forgetting while achieves the fastest post-transition recovery on early tasks. More broadly, our results suggest a scalable continual and meta-learning paradigm for large models and demanding tasks like robotic control. One limitation is our implicit assumption that the task 1 optimum lies close to a shared optimum that also works well for later tasks (see Figure 1c). When tasks are highly heterogeneous, this shared optimum may be far from the task-1 optimum, weakening the benefits of our approach. Future work could study how to identify or construct candidate tasks that are more likely to share a common parameter region for future tasks.

## Impact Statement

This work advances methods for continual learning with meta-learning behavior, making them practical at the scale of modern diffusion backbones and demanding workloads (image generation and robotic control). A key practical benefit is computational efficacy: by relying on rank-1 Fisher approximations, we avoid the substantial overhead of higher-order gradients, thereby improving training throughput Table 6. Faster training directly reduces total GPU-hours and can lower energy consumption and associated environmental impact for researchers who would otherwise require significantly more compute to run comparable experiments. More broadly, scalable continual learning can reduce redundant retraining by enabling a single model to adapt across tasks without catastrophic forgetting, which can further decrease repeated full-training cycles in real-world deployments.

## References

Aljundi, R., Babiloni, F., Elhoseiny, M., Rohrbach, M., and Tuytelaars, T. Memory aware synapses: Learning what (not) to forget. In *Proceedings of the European Conference on Computer Vision (ECCV)*, pp. 139–154, 2018.

Barari, N., Lian, X., and MacLellan, C. J. Robust incremental learning of visual concepts without catastrophic forgetting. *Cognitive Systems Research*, pp. 101447, 2026. ISSN 1389-0417. doi: <https://doi.org/10.1016/j.cogsys.2026.101447>. URL <https://www.sciencedirect.com/science/article/pii/S1389041726000148>.

Chen, J., Wang, Y., Wang, P., Chen, X., Zhang, Z., Lei, Z., and Li, Q. Diffusepast: Diffusion-based generative replay for class incremental semantic segmentation. *arXiv preprint arXiv:2308.01127*, 2023.

Chi, C., Feng, S., Du, Y., Xu, Z., Cousineau, E., Burchfiel, B., and Song, S. Diffusion policy: Visuomotor policy learning via action diffusion. In *Robotics: Science and Systems*, 2023.

Deng, J., Dong, W., Socher, R., Li, L.-J., Li, K., and Fei-Fei, L. Imagenet: A large-scale hierarchical image database. In *Proceedings of the IEEE Conference on Computer Vision and Pattern Recognition (CVPR)*, pp. 248–255, 2009. doi: 10.1109/CVPR.2009.5206848.

Draxler, F., Veschgini, K., Salmhofer, M., and Hamprecht, F. Essentially no barriers in neural network energy landscape. In Dy, J. and Krause, A. (eds.), *Proceedings of the 35th International Conference on Machine Learning*, volume 80 of *Proceedings of Machine Learning Research*, pp. 1309–1318. PMLR, 10–15 Jul 2018.

URL <https://proceedings.mlr.press/v80/draxler18a.html>.

Finn, C., Abbeel, P., and Levine, S. Model-agnostic meta-learning for fast adaptation of deep networks. In *Proceedings of the 34th International Conference on Machine Learning - Volume 70*, ICML’17, pp. 1126–1135. JMLR.org, 2017.

Finn, C., Rajeswaran, A., Kakade, S., and Levine, S. Online meta-learning. In Chaudhuri, K. and Salakhutdinov, R. (eds.), *Proceedings of the 36th International Conference on Machine Learning*, volume 97 of *Proceedings of Machine Learning Research*, pp. 1920–1930. PMLR, 09–15 Jun 2019. URL <https://proceedings.mlr.press/v97/finn19a.html>.

French, R. M. Catastrophic forgetting in connectionist networks. *Trends in Cognitive Sciences*, 3(4):128–135, 1999.

Gao, R. and Liu, W. DDGR: Continual learning with deep diffusion-based generative replay. In Krause, A., Brunskill, E., Cho, K., Engelhardt, B., Sabato, S., and Scarlett, J. (eds.), *Proceedings of the 40th International Conference on Machine Learning*, volume 202 of *Proceedings of Machine Learning Research*, pp. 10744–10763. PMLR, 23–29 Jul 2023. URL <https://proceedings.mlr.press/v202/gao23e.html>.

Garipov, T., Izmailov, P., Podoprikhin, D., Vetrov, D., and Wilson, A. G. Loss surfaces, mode connectivity, and fast ensembling of deep neural networks. In *Advances in Neural Information Processing Systems 31 (NeurIPS 2018)*, pp. 8803–8812, 2018. URL <https://arxiv.org/abs/1802.10026>.

Ghorbani, B., Krishnan, S., and Xiao, Y. An investigation into neural net optimization via hessian eigenvalue density, 2019. URL <https://arxiv.org/abs/1901.10159>.

Goldfarb, D., Evron, I., Weinberger, N., Soudry, D., and Hand, P. The joint effect of task similarity and over-parameterization on catastrophic forgetting: An analytical model. In *International Conference on Learning Representations (ICLR)*, 2024. URL <https://arxiv.org/abs/2401.12617>.

Gupta, G., Yadav, K., and Paull, L. La-maml: Look-ahead meta learning for continual learning, 2020. URL <https://arxiv.org/abs/2007.13904>.

Heng, A. and Soh, H. Selective amnesia: A continual learning approach to forgetting in deep generative models. *Advances in Neural Information Processing Systems*, 36: 17170–17194, 2023.

Heusel, M., Ramsauer, H., Unterthiner, T., Nessler, B., and Hochreiter, S. Gans trained by a two time-scale update rule converge to a local nash equilibrium. In *Advances in Neural Information Processing Systems (NeurIPS)*, 2017.

Ho, J., Jain, A., and Abbeel, P. Denoising diffusion probabilistic models. In *Advances in Neural Information Processing Systems*, 2020.

Hospedales, T., Antoniou, A., Micaelli, P., and Storkey, A. Meta-learning in neural networks: A survey. *arXiv preprint arXiv:2004.05439*, 2020.

Hyvärinen, A. Estimation of non-normalized statistical models by score matching. *Journal of Machine Learning Research*, 6:695–709, 2005.

Janner, M., Du, Y., Tenenbaum, J. B., and Levine, S. Planning with diffusion for flexible behavior synthesis. In *Proceedings of the 39th International Conference on Machine Learning*, 2022.

Javed, K. and White, M. Meta-learning representations for continual learning. In *Advances in Neural Information Processing Systems*, pp. 1818–1828, 2019.

Kim, J., Cho, H., Kim, J., Tiruneh, Y. Y., and Baek, S. Sddgr: Stable diffusion-based deep generative replay for class incremental object detection. In *Proceedings of the IEEE/CVF Conference on Computer Vision and Pattern Recognition (CVPR)*, 2024.

Kingma, D. P. and Ba, J. Adam: A method for stochastic optimization. In *International Conference on Learning Representations (ICLR)*, 2015.

Kirkpatrick, J., Pascanu, R., Rabinowitz, N., Veness, J., Desjardins, G., Rusu, A. A., Milan, K., Quan, J., Ramalho, T., Grabska-Barwinska, A., Hassabis, D., Clopath, C., Kumaran, D., and Hadsell, R. Overcoming catastrophic forgetting in neural networks. *Proceedings of the National Academy of Sciences*, 114(13):3521–3526, March 2017. ISSN 1091-6490. doi: 10.1073/pnas.1611835114. URL <http://dx.doi.org/10.1073/pnas.1611835114>.

Lee, S., Goldt, S., and Saxe, A. Continual learning in the teacher-student setup: Impact of task similarity. In Meila, M. and Zhang, T. (eds.), *Proceedings of the 38th International Conference on Machine Learning*, volume 139 of *Proceedings of Machine Learning Research*, pp. 6109–6119. PMLR, 18–24 Jul 2021. URL <https://proceedings.mlr.press/v139/lee21e.html>.

Li, Z., Zhou, F., Chen, F., and Li, H. Meta-sgd: Learning to learn quickly for few-shot learning. *arXiv preprint arXiv:1707.09835*, 2017.

Martens, J. New insights and perspectives on the natural gradient method. *Journal of Machine Learning Research*, 21(146):1–76, 2020. URL <http://jmlr.org/papers/v21/17-678.html>.

Masip, S., Rodriguez, P., Tuytelaars, T., and Ven, G. M. v. d. Continual learning of diffusion models with generative distillation. In Lomonaco, V., Melacci, S., Tuytelaars, T., Chandar, S., and Pascanu, R. (eds.), *Proceedings of The 3rd Conference on Lifelong Learning Agents*, volume 274 of *Proceedings of Machine Learning Research*, pp. 431–456. PMLR, 29 Jul–01 Aug 2025. URL <https://proceedings.mlr.press/v274/masip25a.html>.

McClelland, J. L., McNaughton, B. L., and O'Reilly, R. C. Why there are complementary learning systems in the hippocampus and neocortex: Insights from the successes and failures of connectionist models. *Psychological Review*, 102(3):419–457, 1995.

McCloskey, M. and Cohen, N. J. Catastrophic interference in connectionist networks: The sequential learning problem. In *Psychology of Learning and Motivation*, volume 24, pp. 109–165. Academic Press, 1989.

Nichol, A. and Dhariwal, P. Improved denoising diffusion probabilistic models. In *Proceedings of the 38th International Conference on Machine Learning (ICML)*, 2021.

Nichol, A., Achiam, J., and Schulman, J. On first-order meta-learning algorithms. *arXiv preprint arXiv:1803.02999*, 2018.

Rebuffi, S.-A., Kolesnikov, A., Sperl, G., and Lampert, C. H. icarl: Incremental classifier and representation learning. In *Proceedings of the IEEE Conference on Computer Vision and Pattern Recognition (CVPR)*, 2017.

Riemer, M., Cases, I., Ajemian, R., Liu, M., Rish, I., Tu, Y., and Tesauro, G. Learning to learn without forgetting by maximizing transfer and minimizing interference. In *International Conference on Learning Representations*, 2019. Poster.

Rolnick, D., Ahuja, A., Schwarz, J., Lillicrap, T. P., and Wayne, G. Experience replay for continual learning, 2019.

Russakovsky, O., Deng, J., Su, H., Krause, J., Satheesh, S., Ma, S., Huang, Z., Karpathy, A., Khosla, A., Bernstein, M., Berg, A. C., and Fei-Fei, L. Imagenet large scale visual recognition challenge. *International Journal of Computer Vision*, 115(3):211–252, 2015. doi: 10.1007/s11263-015-0816-y.

Schulman, J., Levine, S., Moritz, P., Jordan, M. I., and Abbeel, P. Trust region policy optimization, 2017. URL <https://arxiv.org/abs/1502.05477>.

Shin, H., Lee, J. K., Kim, J., and Kim, J. Continual learning with deep generative replay. In *Proceedings of the 31st International Conference on Neural Information Processing Systems*, NIPS'17, pp. 2994–3003, Red Hook, NY, USA, 2017. Curran Associates Inc. ISBN 9781510860964.

Sohl-Dickstein, J., Weiss, E. A., Maheswaranathan, N., and Ganguli, S. Deep unsupervised learning using nonequilibrium thermodynamics. In *Proceedings of the 32nd International Conference on Machine Learning*, volume 37 of *Proceedings of Machine Learning Research*, pp. 2256–2265. PMLR, 2015.

Song, J., Meng, C., and Ermon, S. Denoising diffusion implicit models. In *International Conference on Learning Representations*, 2021a.

Song, Y., Sohl-Dickstein, J., Kingma, D. P., Kumar, A., Ermon, S., and Poole, B. Score-based generative modeling through stochastic differential equations. In *International Conference on Learning Representations*, 2021b. URL <https://openreview.net/forum?id=PxTIG12RRHS>.

van de Ven, G. M. and Tolias, A. S. Generative replay with feedback connections as a general strategy for continual learning, 2019. URL <https://arxiv.org/abs/1809.10635>.

Vincent, P. A connection between score matching and denoising autoencoders. *Neural Computation*, 23(7):1661–1674, 2011. doi: 10.1162/NECO\_a\_00142.

Wang, Z., Gupta, A., Dong, Z., and MacLellan, C. J. Avoid catastrophic forgetting with rank-1 fisher from diffusion models. In *The Fourteenth International Conference on Learning Representations*, 2026. URL <https://openreview.net/forum?id=zCZcbRsc4g>.

Wołczyk, M., Zajkac, M., Pascual-Diaz, S., Szafraniec, M., and Tabor, J. Continual world: A robotic benchmark for continual reinforcement learning. In *Advances in Neural Information Processing Systems (NeurIPS)*, 2021.

Wu, B., Fang, J., Zeng, X., Liang, S., and Zhang, Q. Adaptive compositional continual meta-learning. In *Proceedings of the 40th International Conference on Machine Learning*, volume 202 of *Proceedings of Machine Learning Research*, pp. 37358–37378. PMLR, 2023.

Wu, J., Zhang, Q., and Xu, G. Tiny imagenet challenge. Technical report, Stanford University, 2017. CS231N course report / challenge description.

Wu, Y., Huang, L.-K., Wang, R., Meng, D., and Wei, Y. Meta continual learning revisited: Implicitly enhancing online hessian approximation via variance reduction. In *The Twelfth International Conference on Learning Representations*, 2024. URL <https://openreview.net/forum?id=TpD2aG1h0D>.

Yosinski, J., Clune, J., Bengio, Y., and Lipson, H. How transferable are features in deep neural networks? In *Advances in Neural Information Processing Systems*, 2014.

Yu, T., Quillen, D., He, Z., Julian, R., Hausman, K., Finn, C., and Levine, S. Meta-world: A benchmark and evaluation for multi-task and meta reinforcement learning. In *Proceedings of The Conference on Robot Learning (CoRL)*, volume 100 of *Proceedings of Machine Learning Research*, pp. 1094–1100. PMLR, 2020.

Zenke, F., Poole, B., and Ganguli, S. Continual learning through synaptic intelligence. In *Proceedings of the 34th International Conference on Machine Learning - Volume 70*, ICML'17, pp. 3987–3995. JMLR.org, 2017.

Zverev, D., Koepke, A. S., and Henriques, J. F. On the dangers of bootstrapping generation for continual learning and beyond, 2025.

## A. Full derivation of Equation (12).

We now derive the identity linking Fisher and Hessian using the same notation. Let  $p_\theta(x)$  be the model distribution and define the per-example negative log-likelihood  $\ell(\theta; x) := -\log p_\theta(x)$ . Then

$$g(\theta; x) = \nabla_\theta \ell(\theta; x) = -\nabla_\theta \log p_\theta(x).$$

Consider the Hessian:

$$\begin{aligned} \nabla_\theta^2 \ell(\theta; x) &= -\nabla_\theta^2 \log p_\theta(x) \\ &= -\nabla_\theta \left( \frac{\nabla_\theta p_\theta(x)}{p_\theta(x)} \right) \\ &= -\left( \frac{\nabla_\theta^2 p_\theta(x)}{p_\theta(x)} - \frac{\nabla_\theta p_\theta(x) \nabla_\theta p_\theta(x)^\top}{p_\theta(x)^2} \right) \\ &= \frac{\nabla_\theta p_\theta(x) \nabla_\theta p_\theta(x)^\top}{p_\theta(x)^2} - \frac{\nabla_\theta^2 p_\theta(x)}{p_\theta(x)} \\ &= (\nabla_\theta \log p_\theta(x)) (\nabla_\theta \log p_\theta(x))^\top - \frac{\nabla_\theta^2 p_\theta(x)}{p_\theta(x)}. \end{aligned} \quad (17)$$

Taking expectation over  $x \sim p_\theta$ ,

$$\begin{aligned} \mathbb{E}_{x \sim p_\theta} [\nabla_\theta^2 \ell(\theta; x)] &= \mathbb{E}_{x \sim p_\theta} [(\nabla_\theta \log p_\theta(x)) (\nabla_\theta \log p_\theta(x))^\top] - \mathbb{E}_{x \sim p_\theta} \left[ \frac{\nabla_\theta^2 p_\theta(x)}{p_\theta(x)} \right] \\ &= \mathbb{E}_{x \sim p_\theta} [(\nabla_\theta \log p_\theta(x)) (\nabla_\theta \log p_\theta(x))^\top] - \int \nabla_\theta^2 p_\theta(x) dx \end{aligned} \quad (18)$$

where we used  $\mathbb{E}_{x \sim p_\theta} \left[ \frac{\nabla_\theta^2 p_\theta(x)}{p_\theta(x)} \right] = \int p_\theta(x) \frac{\nabla_\theta^2 p_\theta(x)}{p_\theta(x)} dx = \int \nabla_\theta^2 p_\theta(x) dx$ . Finally, because  $\int p_\theta(x) dx = 1$ ,

$$\int \nabla_\theta^2 p_\theta(x) dx = \nabla_\theta^2 \int p_\theta(x) dx = \nabla_\theta^2 1 = 0. \quad (19)$$

Substituting Equation (19) into Equation (18) and using  $g(\theta; x) = -\nabla_\theta \log p_\theta(x)$  yields

$$\mathbb{E}_{x \sim p_\theta} [\nabla_\theta^2 \ell(\theta; x)] = \mathbb{E}_{x \sim p_\theta} [g(\theta; x) g(\theta; x)^\top],$$

which is exactly Equation (12).

## B. Full derivation of Equation (16)

Let  $\delta_i = \theta - \theta_i^*$ . If  $\theta$  remains in a local neighborhood of  $\theta_i^*$  (trust-region), then a first-order Taylor expansion gives

$$\nabla_\theta \mathcal{L}_{\mathcal{T}_i}(\theta; \tilde{\mathcal{D}}_i) = \nabla_\theta \mathcal{L}_{\mathcal{T}_i}(\theta_i^*; \tilde{\mathcal{D}}_i) + H_i^{\text{te}}(\theta_i^*) \delta_i + \mathcal{O}(\|\delta_i\|^2). \quad (20)$$

Assuming  $\theta_i^*$  is an (approximate) optimum for task  $\mathcal{T}_i$ , the first term is near zero, yielding  $\nabla_\theta \mathcal{L}_{\mathcal{T}_i}(\theta; \tilde{\mathcal{D}}_i) \approx H_i^{\text{te}}(\theta_i^*) \delta_i$ .

The MAML correction term is  $H_i^{\text{tr}}(\theta) \nabla_{\theta'} \mathcal{L}_{\mathcal{T}_i}(\theta'; \mathcal{D}_{\mathcal{T}_i}^{\text{te}})$ . Under the trust-region assumption,  $H_i^{\text{tr}}(\theta) \approx H_i^{\text{tr}}(\theta_i^*)$ . Under replay,  $\tilde{\mathcal{D}}_i$  is generated to match the old-task data distribution, so the query curvature  $H_i^{\text{te}}(\theta_i^*)$  is close to the support curvature  $H_i^{\text{tr}}(\theta_i^*)$ . Thus  $H_i^{\text{tr}}(\theta) \approx H_i^{\text{te}}(\theta_i^*)$ .

For likelihood-based objectives, the empirical Fisher is commonly used as an approximation to the Hessian in expectation, motivating  $H_i^{\text{tr}}(\theta_i^*) \approx H_i^{\text{te}}(\theta_i^*) \approx F^{(i)}(\theta_i^*)$ . Therefore,

$$H_i^{\text{tr}}(\theta) H_i^{\text{te}}(\theta_i^*) \delta_i \approx F^{(i)}(\theta_i^*) F^{(i)}(\theta_i^*) \delta_i = (F^{(i)}(\theta_i^*))^2 \delta_i. \quad (21)$$

If  $F^{(i)}(\theta_i^*)$  is approximately rank-1, write  $F^{(i)}(\theta_i^*) = \rho_i u_i u_i^\top$  with  $\rho_i \geq 0$  and  $\|u_i\| = 1$ . Then

$$(F^{(i)}(\theta_i^*))^2 = (\rho_i u_i u_i^\top)^2 = \rho_i^2 u_i (u_i^\top u_i) u_i^\top = \rho_i^2 u_i u_i^\top = \rho_i (\rho_i u_i u_i^\top) = \rho_i F^{(i)}(\theta_i^*), \quad (22)$$

so  $(F^{(i)}(\theta_i^*))^2 \delta_i \approx \rho_i F^{(i)}(\theta_i^*) \delta_i$ . The scalar  $\rho_i$  is the unique nonzero eigenvalue of  $F^{(i)}(\theta_i^*)$ . Absorbing  $\rho_i$  into the regularizer weight  $\lambda$  (and/or the MAML inner-step  $\alpha$ ) yields an EWC-form term.

## C. Additional Experimental details

### C.1. Task-Incremental Image Generation

#### C.1.1. ADDITIONAL IMPLEMENTATION DETAILS

We adopt a label-conditioned UNet from the *HuggingFace* diffusion library as the denoising model, using default hyperparameters unless otherwise specified. The architecture consists of four ResNet blocks, with 128 output channels in the first downsampling block and 256 output channels in each subsequent block. For sampling, we use a DDIM scheduler with 50 inference steps and 1000 diffusion timesteps. Training hyperparameters are summarized in Table 3. Unless stated otherwise, the same configuration is used across all datasets and tasks.

Table 3. Training configurations used across methods for ImageNet.

Setting	Value
<b>General</b>	
Batch Size	128 (bilevel: 64 support + 64 query)
Optimizer	Adam (Kingma & Ba, 2015) (outer); SGD (inner for bilevel)
Learning Rate	$2 \times 10^{-4}$
Per-task Gradient Update Steps	100 epochs/task
Seeds Averaged	3
<b>EWC</b>	
Fisher Representation	Rank-1 (Wang et al., 2026), estimated over 10,000 samples/task
EWC $\lambda$	15,000
<b>Replay</b>	
Buffer Size per Task	1,300
Replay Ratio	1.0 (bilevel: 1.0)
<b>Meta-learning (bilevel) additional hyperparameters</b>	
Adaptation Steps	1
Inner-loop LR	$1 \times 10^{-4}$
Outer-loop LR	$2 \times 10^{-4}$

#### C.1.2. ADDITIONAL DATASET DETAILS

We use the downsampled **ImageNet-1k** dataset ( $32 \times 32$ ) for computational efficiency while preserving sufficient visual diversity and semantic complexity. Each sample is normalized to  $(-1, 1)$  for diffusion training. We restrict training to the first 500 classes, partitioned into 10 tasks of 50 classes each. Each task contains approximately 64,000 training images. Task splits:  $T_1 = \{0, \dots, 49\}$ ,  $T_2 = \{50, \dots, 99\}$ ,  $\dots$   $T_{10} = \{450, \dots, 499\}$ .

## C.2. Continual Robotic Manipulation

### C.2.1. DIFFUSION POLICY IMPLEMENTATION DETAILS

We implement a 1D conditional diffusion model over action sequences: given an observation history  $o_{1:H}$ , the policy generates an action sequence  $a_{1:T}$ . The denoiser  $\epsilon_\theta$  is a 1D conditional U-Net that operates on the action tensor in channel-first form  $(B, D_a, T)$  and is FiLM-conditioned on a global context vector formed by concatenating (i) a diffusion-timestep embedding and (ii) the flattened observation history of size  $HD_o$ . The timestep embedding has dimension 512 and is produced by a sinusoidal positional encoding followed by a 2-layer MLP (512  $\rightarrow$  2048  $\rightarrow$  512) with Mish activations. The U-Net uses channel widths [256, 512, 1024] with kernel size 5 and GroupNorm (8 groups): the encoder has 3 resolution stages, each with two FiLM-conditioned residual Conv1D blocks plus a strided downsampling layer (except the last stage); the bottleneck has 2 additional residual blocks; and the decoder has 2 upsampling stages with skip connections, each with two residual blocks and transposed-convolution upsampling, followed by a final Conv1D block and a  $1 \times 1$  projection back to  $D_a$ . Overall, the noise-prediction network contains 12 FiLM-conditioned residual blocks, and we add multi-head self-attention (8 heads) at U-Net levels 2 and 3 (the 512- and 1024-channel resolutions). For the diffusion process we use a DDIM scheduler with 1000 training timesteps and run 50 denoising steps at inference. Training hyperparameters are summarized in Table 4

Table 4. Training configurations used across methods for Meta-World CW10.

Setting	Value
<b>General</b>	
Batch Size	256 (bilevel: 128 support + 128 query; effective 256)
Optimizer	Adam (Kingma & Ba, 2015) (outer); SGD (inner for bilevel)
Learning Rate	$2 \times 10^{-4}$
Per-task Update Steps	50,000 (gradient / meta-updates)
Seeds Averaged	4
<b>EWC</b>	
Fisher Representation	Rank-1 (Wang et al., 2026), estimated over 20,000 training samples/task
EWC $\lambda$	12
<b>Replay</b>	
Buffer Size per Task	2,500 rollouts/task
Replay Ratio	1.0 (bilevel: 1.0)
<b>Meta-learning (bilevel) additional hyperparameters</b>	
Adaptation Steps	1
Inner-loop LR	$1 \times 10^{-4}$
Outer-loop LR	$2 \times 10^{-4}$

### C.2.2. ADDITIONAL TASK AND DATASET DETAILS

We evaluate on a 10-task continual manipulation sequence (CW10) derived from Meta-World. All tasks share a common low-dimensional state representation and continuous control interface, enabling transfer across tasks.

We use low-dimensional, goal-conditioned state observations  $o_t \in \mathbb{R}^{39}$  and continuous actions  $a_t \in \mathbb{R}^4$ . Following the standard Meta-World state interface, the 4D action consists of a desired end-effector displacement in  $\mathbb{R}^3$  and a 1D gripper control. The 39D observation includes end-effector state, gripper state, object pose information, and goal information (shared across tasks). For diffusion policy training, we linearly rescale each action dimension to  $[-1, 1]$  (and clip to the same range at training and sampling time) to keep the action domain bounded and consistent across tasks.

Episodes use a fixed horizon of maximum 200 environment steps. We report success rate, defined as the fraction of evaluation rollouts that satisfy the task-specific success condition.

**Task suite.** Each task shares the same observation/action interface but requires a distinct manipulation skill:

- **hammer-v1** — The agent uses a hammer to drive a nail into a wall.
- **push-wall-v1** — The agent pushes a block toward a designated target position on a wall.
- **faucet-close-v1** — The agent rotates a faucet handle clockwise to close it.
- **push-back-v1** — The agent pushes an object backward to a specified target location.
- **stick-pull-v1** — The agent grasps a stick tool and uses it to pull an object toward a target region.
- **handle-press-side-v1** — The agent presses a handle on an appliance from the side.
- **push-v1** — The agent pushes an object to a specified target position.
- **shelf-place-v1** — The agent picks up an object and places it onto a shelf.
- **window-close-v1** — The agent closes a window by manipulating the window or its handle.
- **peg-unplug-side-v1** — The agent unplugs a peg from a socket by pulling it out from the side.

### C.2.3. DIFFUSION POLICY DATA REPRESENTATION

We conduct a small grid search over three sequence-encoding hyperparameters for the CW10 diffusion policy: sequence length  $S$ , observation horizon  $O$ , and action chunk size  $A$ . To isolate the effect of these design choices, we use the *same model architecture and training configuration* as in our continual learning experiments, except that we train *one model per task from scratch* (i.e., no task sequence and no continual updates), and then report the average success rate across the 10 CW10 tasks.

As shown in Table 5, the configuration  $(S, O, A) = (8, 6, 2)$  achieves the highest mean success rate (0.859), improving over the next best setting  $(8, 8, 1)$  (0.808). We therefore adopt  $S=8$ ,  $O=6$ , and  $A=2$  as the default CW10 diffusion policy configuration in all main continual learning experiments.

*Table 5.* CW10 diffusion policy configuration grid search results. We report the mean success rate across 10 tasks. Higher is better. Each configuration is trained from scratch separately for each task, using the same model and training setup as in our continual learning experiments.

Config	$S$	$O$	$A$	Mean success $\uparrow$
<b>S8_O6_A2</b>	8	6	2	<b>0.859</b>
S8_O8_A1	8	8	1	0.808
S8_O4_A4	8	4	4	0.744
S8_O4_A2	8	4	2	0.622
S16_O8_A8	16	8	8	0.511
S16_O8_A4	16	8	4	0.486
S16_O12_A4	16	12	4	0.449
S16_O16_A1	16	16	1	0.326
S32_O16_A4	32	16	4	0.184
S32_O24_A4	32	24	4	0.177
S32_O16_A8	32	16	8	0.121
S32_O16_A16	32	16	16	0.081
S32_O24_A8	32	24	8	0.034

### C.3. Compute Efficacy

Our models are  $34\text{--}76\times$  larger and use substantially larger batches than the original VR-MCL setting (Wu et al., 2024), making full second-order hypergradients impractical at our target scale (second-order reduces throughput from  $\sim 5$  it/s to  $\sim 1$  it/s, i.e.,  $\approx 5\times$  slower) (See Table 6). Nevertheless, the first-order meta-learning baselines remain scalable and allow us to evaluate variance-reduction and continual-learning behavior under a matched compute budget. Table 7 reports the average runtime for each dataset and method (using first order), including evaluation.

## D. Additional Results

### D.1. Imagenet Per Task Re-Convergence Tables

We present the re-convergence tables for all Imagenet tasks Tables 8 to 15.

### D.2. CW10 Per Task Re-Convergence Tables

We present the re-convergence tables for all CW10 tasks Tables 16 to 23

Table 6. Model scale and training throughput. Our diffusion backbones are substantially larger than the reduced ResNet used in VR-MCL, and we report the resulting training speed under our first-order implementation versus a second-order (higher-order autodiff) variant.

Setting	Backbone	Params (M)	$\times$ vs. 1.09M	Batch size	it/s (FO)	it/s (2nd)
ImageNet diffusion	UNet	37.45	34.4 $\times$	128	$\sim$ 5	$\sim$ 1
CW10 diffusion policy	UNet	83.27	76.4 $\times$	256	$\sim$ 5	$\sim$ 1
VR-MCL from (Wu et al., 2024)	reduced ResNet	1.09	1.0 $\times$	32	—	—

Table 7. Average training runtime (hours) and GPU used per dataset/method.

Evaluation	Method	Hours	GPU
CW10	Continual Finetuning	$\sim$ 21	NVIDIA A40
CW10	EWC	$\sim$ 29	NVIDIA A40
CW10	Replay	$\sim$ 22	NVIDIA A40
CW10	Trust Region	$\sim$ 31	NVIDIA A40
CW10	FTML	$\sim$ 29	NVIDIA A40
CW10	VRMCL	$\sim$ 41	NVIDIA A40
ImageNet	Continual Finetuning	$\sim$ 12	NVIDIA H200
ImageNet	EWC	$\sim$ 15	NVIDIA H200
ImageNet	Replay	$\sim$ 22	NVIDIA H200
ImageNet	Trust Region	$\sim$ 31	NVIDIA H200
ImageNet	FTML	$\sim$ 29	NVIDIA H200
ImageNet	VRMCL	$\sim$ 44	NVIDIA H200

Imagenet-500																							
Method	+10%					+20%					+30%					T3	T4	T5	T6	T7	T8	T9	T10
	T3	T4	T5	T6	T7	T8	T9	T10	T3	T4	T5	T6	T7	T8	T9	T10							
Finetune	76	—	—	—	—	—	—	—	26	—	—	—	41	—	—	—	16	—	—	—	41	—	—
EWC	—	—	—	—	—	—	—	—	66	—	—	—	9001	—	—	—	56	—	—	—	7001	—	—
Replay	—	—	—	—	—	—	—	—	91	—	—	—	—	—	—	—	71	3001	—	—	—	—	—
FTML	—	—	—	—	—	—	—	—	41	36	—	—	—	—	—	—	21	21	—	—	—	—	—
VRMCL	—	—	—	—	—	—	—	—	26	—	—	—	—	—	—	—	26	—	—	—	—	—	—
Trust Region	56	—	—	—	—	—	—	—	16	56	—	—	—	—	—	—	16	51	51	—	76	—	—

Table 8. Steps to re-converge Task 2 under continual learning for Imagenet.

Imagenet-500																						
Method	+10%					+20%					+30%					T4	T5	T6	T7	T8	T9	T10
	T4	T5	T6	T7	T8	T9	T10	T4	T5	T6	T7	T8	T9	T10	T4	T5	T6	T7	T8	T9	T10	
Finetune	—	—	—	—	—	—	—	—	—	—	—	—	—	—	—	—	—	—	—	—	—	
EWC	—	—	—	—	—	—	—	—	—	—	—	—	—	—	—	—	—	—	—	—	—	
Replay	701	—	—	—	—	—	—	351	—	—	—	—	—	—	96	—	—	—	—	—	—	
FTML	—	—	—	—	—	—	—	—	—	—	—	—	—	—	—	26	—	—	—	—	—	—
VRMCL	—	—	—	—	—	—	—	—	451	—	—	—	—	—	—	71	—	—	—	—	—	—
Trust Region	31	51	56	76	—	—	—	31	26	41	46	—	—	—	11	26	36	31	66	41	—	

Table 9. Steps to re-converge Task 3 under continual learning for Imagenet.

Imagenet-500																						
Method	+10%					+20%					+30%					T5	T6	T7	T8	T9	T10	
	T5	T6	T7	T8	T9	T10	T5	T6	T7	T8	T9	T10	T5	T6	T7	T8	T9	T10	T5	T6	T7	
Finetune	—	—	—	—	—	—	—	—	—	—	—	—	—	—	—	—	—	—	—	—	—	
EWC	—	—	—	—	—	—	—	—	—	—	—	—	—	—	—	—	—	—	—	—	—	
Replay	—	—	—	—	—	—	—	—	—	—	—	—	—	—	—	—	—	—	—	—	—	
FTML	—	—	—	—	—	—	—	—	—	—	—	—	—	—	—	26	—	—	—	—	—	—
VRMCL	40001	—	—	—	—	—	—	9001	—	—	—	—	—	—	—	6	46	—	—	—	—	—
Trust Region	—	—	—	—	—	—	—	—	—	—	—	—	—	—	—	—	—	—	—	—	—	—

Table 10. Steps to re-converge Task 4 under continual learning for Imagenet.

## Trust-Region CL as an Implicit Meta-Learner

Method	Imagenet-500													
	+10%					+20%					+30%			
	T6	T7	T8	T9	T10	T6	T7	T8	T9	T10	T6	T7	T8	T9
Finetune	—	—	—	—	—	—	—	—	—	—	—	—	—	—
EWC	—	—	—	—	—	—	—	—	—	—	—	—	—	—
Replay	46	—	—	—	—	2	201	—	—	—	2	71	—	—
FTML	—	—	—	—	—	—	—	—	—	—	8	—	—	—
VRMCL	—	—	—	—	—	—	—	—	—	—	—	—	—	—
Trust Region	701	—	—	—	—	51	951	—	—	—	41	551	—	—

Table 11. Steps to re-converge Task 5 under continual learning for Imagenet.

Method	Imagenet-500											
	+10%					+20%					+30%	
	T7	T8	T9	T10	T7	T8	T9	T10	T7	T8	T9	T10
Finetune	—	—	—	—	—	—	—	—	—	—	—	—
EWC	—	—	—	—	—	—	—	—	—	—	—	—
Replay	—	—	—	—	—	—	—	—	—	—	—	—
FTML	—	—	—	—	—	—	—	—	—	—	—	—
VRMCL	—	—	—	—	—	—	—	—	—	—	—	—
Trust Region	—	—	—	—	—	—	—	—	—	—	—	—

Table 12. Steps to re-converge Task 6 under continual learning for Imagenet.

Method	Imagenet-500											
	+10%			+20%			+30%					
	T8	T9	T10	T8	T9	T10	T8	T9	T10	T8	T9	T10
Finetune	—	—	—	—	—	—	—	—	—	2	—	—
EWC	—	—	—	56	—	—	46	—	—	—	—	—
Replay	31	—	—	26	551	—	8	151	56	—	—	—
FTML	—	—	—	46	—	—	36	—	—	—	—	—
VRMCL	—	—	—	61	—	—	46	—	—	—	—	—
Trust Region	66	2001	8001	56	61	51	56	41	26	—	—	—

Table 13. Steps to re-converge Task 7 under continual learning for Imagenet.

Method	Imagenet-500											
	+10%		+20%		+30%							
	T9	T10	T9	T10	T9	T10	T9	T10	T9	T10	T9	T10
Finetune	—	—	—	—	—	—	4	—	—	—	—	—
EWC	—	—	—	—	—	—	—	—	—	—	—	—
Replay	851	—	501	401	151	66	—	—	—	—	—	—
FTML	—	—	—	—	—	—	7001	—	—	—	—	—
VRMCL	—	—	—	—	—	—	—	—	—	—	—	—
Trust Region	2001	8001	851	551	41	51	—	—	—	—	—	—

Table 14. Steps to re-converge Task 8 under continual learning for Imagenet.

Method	Imagenet-500											
	+10%		+20%		+30%							
	T10	T10	T10	T10	T10	T10	T10	T10	T10	T10	T10	T10
Finetune	16	2	2	2	—	—	—	—	—	—	—	—
EWC	66	51	16	—	—	—	—	—	—	—	—	—
Replay	4	2	2	2	—	—	—	—	—	—	—	—
FTML	11	8	8	8	—	—	—	—	—	—	—	—
VRMCL	—	201	81	—	—	—	—	—	—	—	—	—
Trust Region	26	21	16	—	—	—	—	—	—	—	—	—

Table 15. Steps to re-converge Task 9 under continual learning for Imagenet.

## Trust-Region CL as an Implicit Meta-Learner

Method	CW10																							
	99%									90%						80%								
	T3	T4	T5	T6	T7	T8	T9	T10	T3	T4	T5	T6	T7	T8	T9	T10	T3	T4	T5	T6	T7	T8	T9	T10
Finetune	—	—	—	—	—	—	—	—	—	—	—	—	—	—	—	—	—	—	—	—	—	—	—	
EWC	—	—	—	—	—	—	—	—	—	—	—	—	—	—	—	—	—	—	—	—	—	—	—	
Replay	76	46	41	31	5001	751	9001	10001	21	21	21	16	4	46	4	16	10	4	6	4	4	21	4	4
FTML	4000	—	550	—	—	—	—	—	3000	250	95	60	4	—	40	—	3000	70	60	55	4	70	4	6
VRMCL	40000	30000	—	—	—	—	—	—	200	60	150	80	4	200	8	35	4	30	150	6	4	75	6	8
Trust Region	151	61	46	4	5001	41	4	6	10	26	16	4	11	21	4	6	8	4	16	4	4	16	4	4

Table 16. Steps to re-converge Task 2 under continual learning for CW10.

Method	CW10																				
	99%							80%							70%						
	T4	T5	T6	T7	T8	T9	T10	T4	T5	T6	T7	T8	T9	T10	T4	T5	T6	T7	T8	T9	T10
Finetune	—	—	—	5000	—	10000	—	—	—	—	4000	—	7000	—	4000	—	—	3000	—	6000	—
EWC	—	—	—	—	—	—	—	—	—	—	—	—	—	—	—	—	—	—	—	—	—
Replay	21	4	4	4	6	4	26	4	4	4	4	4	4	8	4	4	4	4	4	4	6
FTML	35	65	4	4	35	15	35	4	4	4	4	10	4	8	4	4	4	4	4	4	6
VRMCL	95	400	40	4	40	500	150	20	4	4	4	4	8	45	20	4	4	4	4	8	8
Trust Region	16	4	4	4	6	4	16	4	4	4	4	4	4	6	4	4	4	4	4	4	6

Table 17. Steps to re-converge Task 3 under continual learning for CW10.

Method	CW10																	
	99%					90%					80%							
	T5	T6	T7	T8	T9	T10	T5	T6	T7	T8	T9	T10	T5	T6	T7	T8	T9	T10
Finetune	—	—	—	—	—	—	—	—	—	—	—	—	—	—	—	—	—	
EWC	—	—	—	—	—	—	—	—	—	—	—	—	—	—	—	—	—	
Replay	36	21	4	8	4	21	10	16	4	8	4	8	8	11	4	4	4	
FTML	300	55	20	80	—	600	80	50	20	80	4	20	55	50	10	20	4	20
VRMCL	55	40	40	50	4	—	6	40	8	50	4	—	6	30	8	15	4	75
Trust Region	21	16	4	61	4	16	21	16	4	10	4	6	8	10	4	4	4	6

Table 18. Steps to re-converge Task 4 under continual learning for CW10.

Method	CW10														
	99%					90%					80%				
	T6	T7	T8	T9	T10	T6	T7	T8	T9	T10	T6	T7	T8	T9	T10
Finetune	-	-	-	-	-	-	-	-	-	-	-	-	-	-	-
EWC	-	-	-	-	-	-	-	-	-	-	-	-	-	-	-
Replay	31	6	451	71	76	31	6	31	51	41	26	6	31	4	4
FTML	-	-	-	-	-	9000	50	-	-	-	550	40	-	-	-
VRMCL	-	-	-	-	-	7000	10	-	-	-	2000	10	2000	-	350
Trust Region	96	91	6001	76	301	86	10	51	16	4	51	6	31	4	4

Table 19. Steps to re-converge Task 5 under continual learning for CW10.

Table 20. Steps to re-converge Task 6 under continual learning for CW10.

Method	CW10									
	99%			90%			80%			
	T8	T9	T10	T8	T9	T10	T8	T9	T10	
Finetune	—	—	—	—	—	—	—	—	—	—
EWC	—	—	—	—	—	—	—	—	—	—
Replay	51	21	36	10	4	4	10	4	4	
FTML	550	550	—	60	6	30	40	4	6	
VRMCL	2000	75	—	55	6	—	30	4	45	
Trust Region	41	4	36	21	4	4	10	4	4	

Table 21. Steps to re-converge Task 7 under continual learning for CW10.

Method	CW10					
	99%		90%		80%	
	T9	T10	T9	T10	T9	T10
Finetune	—	—	—	—	—	—
EWC	—	—	—	—	—	—
Replay	36	2001	4	86	4	4
FTML	65	—	45	—	6	500
VRMCL	—	—	8000	550	4	350
Trust Region	96	—	4	71	4	4

Table 22. Steps to re-converge Task 8 under continual learning for CW10.

Method	CW10		
	99%		90%
	T10	T10	T10
Finetune	—	—	30
EWC	30	30	30
Replay	4	4	4
FTML	4	4	4
VRMCL	550	75	10
Trust Region	4	4	4

Table 23. Steps to re-converge Task 9 under continual learning for CW10.